JOURNAL OF GEOPHYSICAL RESEARCH, VOL. 104, NO. C9, PAGES 20,911–20,926, SEPTEMBER 15, 1999

On the crossing of the equator by intermediate water masses in the western Atlantic ocean: Identification and pathways of Antarctic Intermediate Water and Upper Circumpolar Water

C. Oudot,[1] J. F. Ternon,[2] C. Andrié,[3] E. S. Braga,[4] and P. Morin[5]

Abstract. The flow of intermediate water masses across the equator in the Atlantic Ocean is of fundamental interest in the context of the global meridional circulation cell associated with the formation of the North Atlantic Deep Water. This paper describes the flow and pathways of the Antarctic Intermediate Water (AAIW) and the Upper Circumpolar Water (UCPW) at between 500- and 1200-m depths in the western equatorial Atlantic (5°S – 7°30'N). These have been deduced from hydrological and geochemical tracer (nutrients and chlorofluorocarbons) data sets from CITHER 1 (R/V *L'Atalante*, January-March 1993), ETAMBOT 1 (R/V *Le Noroit*, September-October 1995), and ETAMBOT 2 (R/V *Edwin Link*, April-May 1996) cruises. Both the AAIW and UCPW enter, on the isopycnals $\sigma_\theta = 27.25$ (676 ± 36 dbar) and $\sigma_\theta = 27.40$ (919 ± 35 dbar), respectively, the equatorial belt as narrow, northwestward flows around the northeast tip of Brazil near 5°S. During transit within this zone the core properties of UCPW erode more than those of AAIW. Flow patterns of both the water masses show westward spreading and eastward recirculations on either side of the equator. Temporal variations in spreading and recirculation occur at both levels, but they are more pronounced at the AAIW level, in agreement with earlier observations in the upper layers. At the northern boundary of the equatorial belt (7°30'N) the AAIW flows along the western boundary while the UCPW, instead, recirculates into the interior of the ocean.

1. Introduction

In the conveyor belt model of the world ocean thermohaline circulation, the export of cold North Atlantic Deep Water (NADW) is balanced by an import of warm waters from the upper layers, including the intermediate waters [*Gordon*, 1986; *Rintoul*, 1991; *Gordon et al.*, 1992]. In the Atlantic the major intermediate water mass is the Antarctic Intermediate Water (AAIW), of subantarctic origin and flowing northward [*Wüst*, 1935]. Conversion of intermediate water into warmer thermocline water at the equatorial crossing is probably the reason for its northward transport within the upper limb of the thermohaline cell in the North Atlantic [*Schmitz and Richardson*, 1991]. Geostrophic inverse modeling (M. Lux et al., Interhemispheric exchanges of mass and heat in the Atlantic ocean in January-March 1993, submitted to *Deep Sea Research Part I*, 1999) also predicts a convective cell south of the equator and conversion of the intermediate water into upper NADW. These inherently complex exchanges between the intermediate waters and the overlying warm waters, on one hand, and the underlying cold waters, on the other hand, occur mainly in the western equatorial Atlantic. However, notwithstanding the importance of the intermediate water to the thermohaline circulation between the North and South Atlantic Oceans, this layer, except for a few recent studies [*Suga and Talley*, 1995; *Bub and Brown*, 1996], has received little attention.

The northward spreading AAIW can be traced by its salinity minimum accompanied by a high-oxygen anomaly [*Wüst*, 1935]. The oxygen maximum disappears as it meets the strong oxygen minimum characteristic of the equatorial zone [*Reid*, 1989]. Just beneath the salinity minimum in the lower part of the intermediate layer there is a potential temperature minimum that has been identified by *Reid* [1989] as the signature of the Upper Circumpolar Water (UCPW). Thus the AAIW and UCPW constitute the deepest layer of the relatively warm Atlantic waters. The equatorial circulation within this layer, lying approximately between 500 and 1200 m, differs from that of the overlying South Atlantic Central Water layer [*Stramma and Schott*, 1996]. The trajectories of the floats at 800 m depth in the study of *Richardson and Schmitz* [1993] also reveal the complex pathways of the water masses in the western tropical Atlantic. Nevertheless, in the equatorial Atlantic, the AAIW and UCPW are often treated as a single layer [*Stramma and Schott*, 1996], and even now the circulation of UCPW has not been differentiated from that of the AAIW. For example, *Tsuchyia et al.* [1994] consider the temperature minimum and the associated silicate maximum north of 21°S as the lower boundary of the AAIW rather than the northward extension of the UCPW silicate maximum.

[1] Institut de Recherches pour le Développement, Plouzané, France.
[2] Institut de Recherches pour le Développement, Cayenne, French Guiana.
[3] Laboratoire d'Océanographie Dynamique et de Climatologie, Paris.
[4] Instituto Oceanográfico da Universidade de São Paulo, São Paulo.
[5] Centre National de la Recherche Scientifique, Roscoff, France.

Paper number 1999JC900123.
0148-0227/99/1999JC900123$09.00

The large amount of data, in particular, on the geochemical (nutrients and chlorofluorocarbons) tracers, collected during the trans-Atlantic CITHER 1 cruise on World Ocean Circulation Experiment Hydrographic Programme (WHP) lines A6 and A7 and the ETAMBOT cruises in the western equatorial Atlantic, gave us an opportunity to study and differentiate the circulation patterns of AAIW and UCPW in the equatorial Atlantic, especially on its western boundary. The two trans-Atlantic Conductivity-temperature-depth-oxygen ($CTDO_2$) tracer sections with closely spaced stations along 7°30'N and 4°30'S (WHP lines A6 and A7) and the two meridional sections along 3°50'W and 35°W between these two latitudes were occupied in January-March 1993 (CITHER 1 cruise; Figure 1a) [*Andrié et al.*, 1998; *Arhan et al.*, 1998; *Oudot et al.*, 1998]. The western equatorial Atlantic basin stations of the CITHER 1 cruise were reoccupied twice, together with a new short internal section (0°, 45° W to 8°30'N, 41°W; Figure 1b), during the ETAMBOT 1 (September-October 1995) and ETAMBOT 2 (April-May 1996) cruises. The ETAMBOT program was designed to investigate temporal variations in a region where a large variability of the circulation is well known from the surface layer and suspected at depth. It completes, at the intermediate water level, the recent Western Tropical Atlantic Experiment (WESTRAX) surveys [*Bub and Brown*, 1996] between 12-14°N and 44°W and *Meteor* surveys [*Schott et al.*, 1995, 1998] between 10°S and 44°W. Thus, using the CITHER 1 and ETAMBOT data sets, this paper documents the circulation patterns of AAIW and UCPW in the western equatorial Atlantic and the temporal variability expected in the intermediate layer. This is in consonance with the seasonal variations observed in the upper layers during WESTRAX

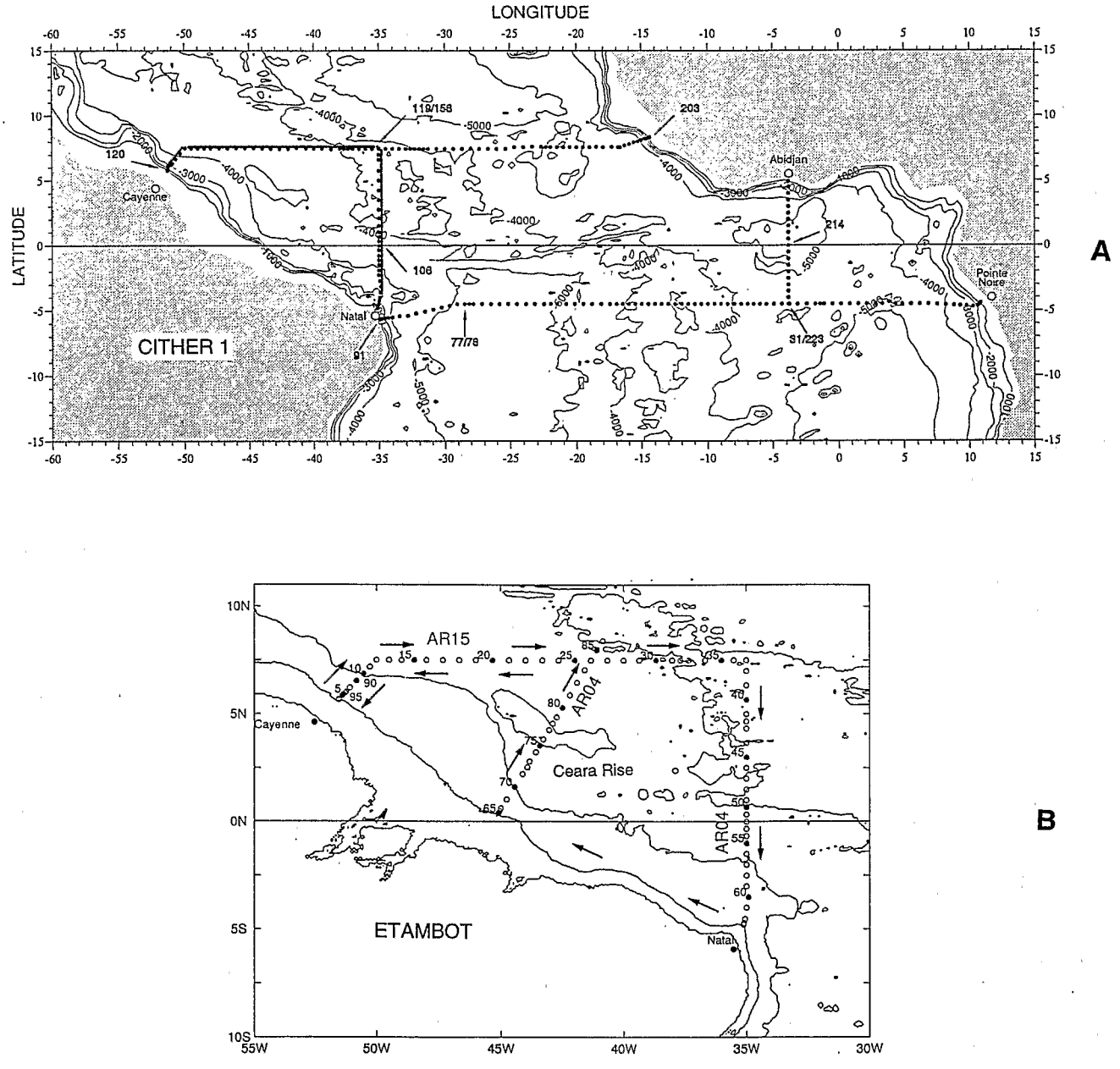

Figure 1. Tracks of (a) CITHER 1 (January–March 1993) and (b) ETAMBOT 1 (September–October 1995) and ETAMBOT 2 (April–May 1996).

[*Brown et al.*, 1992; *Bourlès et al.*, 1999], France WOCE (*Bourlès et al.*, this issue], and Germany WOCE projects [*Stramma and Schott*, 1996] and predicted by numerical models [*Schott and Böning*, 1991; *Didden and Schott*, 1992].

This paper presents, in sequence, the following: the data set, the characteristic properties of AAIW and UCPW at their sources and in the equatorial region, and the relative proportions of both these intermediate water masses, their pathways, and temporal variations in them at the latter site. The interpretation of the results is strengthened with data from simultaneous acoustic Doppler current profiler (ADCP) current measurements and/or vertical oscillations of the isopycnal surfaces, in addition to the historical data sets.

2. Data Set and Methods

To recapitulate, the data used in this paper were obtained during the CITHER 1 (R/V *L'Atalante*, January-March 1993), ETAMBOT 1 (R/V *Le Noroit*, September-October 1995), and ETAMBOT 2 (R/V *Edwin Link*, April-May 1996) cruises (Figure 1). About 75% of the stations occupied during the ETAMBOT cruises were duplicates of the western Atlantic CITHER 1 stations (joined by a solid line in Figure 1a). Within the western equatorial Atlantic a short oblique section, from 0°, 45°W to 8°30'N, 41°W, across the Ceara Rise (hereinafter referred to as the Ceara section) was also occupied during the ETAMBOT cruises (Figure 1b).

Methods of data acquisition from $CTDO_2$ casts and onboard laboratory analyses for other geochemical tracers [*Andrié et al.*, 1998; *Arhan et al.*, 1998; *Oudot et al.*, 1998] were the same in all three cruises, except that the depths sampled in a single hydrocast during the ETAMBOT cruises were 22, compared with 32 in the CITHER 1 cruise, with the remaining space in the 24-bottle rosette (General Oceanics™) used for the mounting of a lowered ADCP (LADCP) current profiler [*Bourlès et al.*, this issue; *Gouriou et al.*, this issue]. However, the vertical resolution at the deepest stations (depth >4000 m) during the ETAMBOT cruises was increased by resorting to double hydrocasts, covering a total of 28 depths.

The precisions (1 standard deviation) for temperature and salinity measurements, both from CTD profiles and of discrete samples, were 0.005°C and 0.003, respectively. The precision of dissolved oxygen measurements with the sensor (1.5 µmol kg^{-1}, i.e., 0.034 mL L^{-1}) was not as good as that from Winkler analyses (0.5 µmol kg^{-1}, i.e. 0.011 mL L^{-1}). Analytical precision for nutrients, calculated from measurements of more than 70 duplicate samples and at seven test (all bottles fired at a predetermined depth) stations (three stations in ETAMBOT 1 and four in ETAMBOT 2), 0.2 µmol kg^{-1} for silicate, 0.1 µmol kg^{-1} for nitrate, and 0.02 µmol kg^{-1} for phosphate, was the same as in the CITHER 1 cruise. Phosphate data from all three cruises also confirmed the underestimate of the CITHER 1 results (about 0.03 µmol kg^{-1}), compared with the historical data [*Oudot and Baurand*, 1994]. Details of analytical methods and precision (<1%) for the measurements of the transient tracers CFC-11 and CFC-12 are reported elsewhere in this special section [*Andrié et al.*, this issue]. Though both CFC-11 and CFC-12 were measured at all stations, only the data on CFC-11 are reported here. This choice was dictated by the facts that one of the intermediate waters is characterized by low CFC concentrations and the analytical precision obtained with CFC-11, more soluble than the other, was better.

Ship-mounted ADCP (SADCP) profiles were obtained along the tracks of all three cruises, but only in the CITHER 1 cruise did the SADCP profiles reach the depth of the intermediate waters [*Gouriou et al.*, 1994]. The uncertainty in the mean SADCP profiles was of the order of 3 cm s^{-1} [*Bourlès et al.*, this issue]. During both ETAMBOT cruises it was planned to obtain LADCP profiles from surface to bottom at each hydrographic station, but only 33 such profiles along the 7°30'N section during the first leg of ETAMBOT 1 could be obtained [*Chuchla et al*, 1997a, b]. During ETAMBOT 2, however, LADCP profiles were obtained at all hydrographic stations (89 profiles). The difficulties in the evaluation of the precision of LADCP measurements are discussed by *Gouriou et al.* [this issue].

In the present study the potential temperature and geochemical tracer concentrations at the core isopycnal surfaces (σ_θ = 27.25 and 27.40, respectively) of AAIW (salinity and oxygen) and UCPW (potential temperature and silicate) were obtained from linear interpolation of the discrete data.

3. Characterization of AAIW and UCPW

These two intermediate water masses originate from different source areas and acquire hydrographic and geochemical properties that enable a clear differentiation between the two at the start.

3.1. Sources of AAIW and UCPW in the Southern Ocean

The AAIW forms in the Subantarctic Front region (45°S) and propagates northward into the South Atlantic as a low-salinity, oxygenated and CFC-enriched tongue, below the thermocline layer, at between 500- and 1000-dbar pressures [*Wüst*, 1935; *Reid*, 1989; *Gordon et al.*, 1992; *Warner and Weiss*, 1992; *Tsuchiya et al.*, 1994; *Suga and Talley*, 1995]. *Talley* [1996] distinguishes two types of AAIW, both formed by pycnostad subduction: one is produced west of Drake Passage and enters the South Atlantic within the Antarctic Circumpolar Current and the other is produced east of Drake Passage, in the confluence of the Falkland and Brazil Currents [see *Maamaatuaiahutapu et al.*, this issue]. The transport of AAIW in the South Atlantic is mostly driven by the anticyclonic subtropical gyre and the AAIW flow crosses the equator along the western boundary [*Wüst*, 1935; *Reid*, 1989, 1994; *Warner and Weiss*, 1992; *Boebel et al.*, 1997; *Larqué et al.*, 1997]. *Suga and Talley* [1995] also identify two eastward extending, low-salinity branches of AAIW on either side (3-4°S and 1-2°N) of the equator.

A silicate maximum has often been considered as indicative of the presence of AAIW in the North Atlantic [*Wüst*, 1935; *Metcalf*, 1969; *Mann et al.*, 1973; *Tsuchiya*, 1989; *Tsuchiya et al.*, 1992]. However, in the South Atlantic, this silicate maximum, lying near the 1000-dbar pressure level [*Reid*, 1989] and traceable southward up to the Polar Front (50°S) [*Tsuchiya et al.*, 1994], clearly characterizes the UCPW that lies below AAIW. The coincidence of the silicate maximum along with the temperature-oxygen minimum led *Reid* [1989] to hypothesize that the UCPW originates from a source different from the oxygen-rich surface layer source of AAIW. The UCPW, unlike the AAIW, which

originates in silicon-poor surface waters, derives its high silicon content from an admixture of silica-rich Pacific and Antarctic waters [*Talley*, 1996]. The deep water origin of UCPW is also evident in the association of a CFC-11 minimum with the UCPW core, identifiable by an oxygen minimum layer between the AAIW and the upper NADW (UNADW) at 19°S in the Brazil Basin [*Wallace et al.*, 1994]. However, farther north, the UCPW progressively loses, as it meets the overlying oxygen-poor and phosphate-rich equatorial water, the identity of its nonconservative characteristics (oxygen and nutrients), retaining only the silicate maximum that can be traced in the North Atlantic. The equatorial water is less enriched in silicon than the southern water, because silicate-utilizing organisms are far less abundant in the tropics than in polar waters; the southern silicate maximum hence does not merge with the equatorial one, as occurs with the phosphate maximum.

3.2. Identification of AAIW Near the Equator

The AAIW becomes clearly distinguishable as a vertical salinity minimum (Figure 2a) and oxygen maximum (Figure 2b) in the 500- to 1500-dbar layer on the 4°30'S CITHER 1 transect [*Arhan et al.*, 1998]. The extrema are located at about the σ_θ =

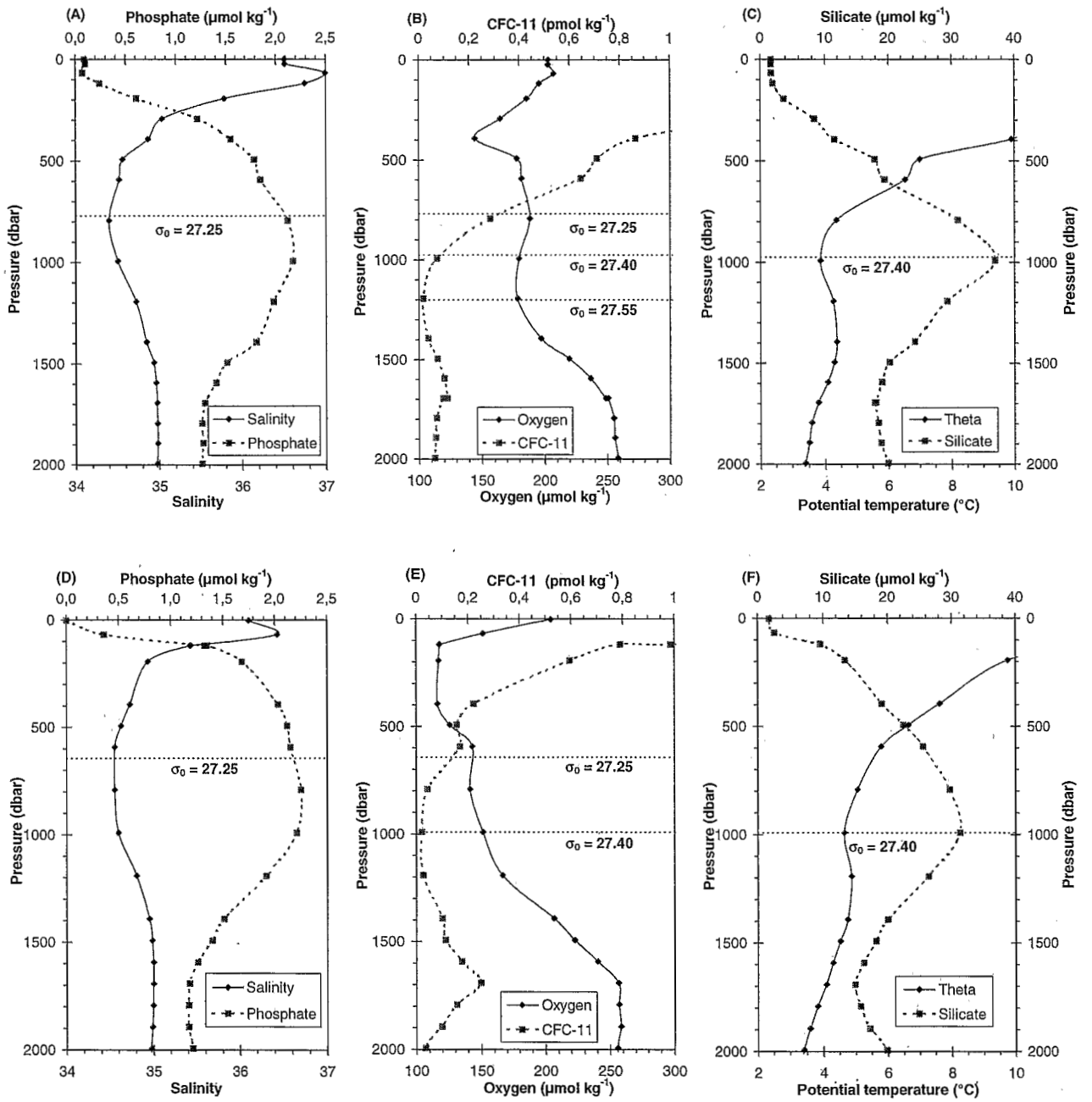

Figure 2. Vertical distributions of (a) salinity and phosphate, (b) oxygen and CFC-11, and (c) potential temperature (θ) and silicate at the station south of the equator (5°38'S, 34°49'W) and (d) salinity and phosphate, (e) oxygen and CFC-11, and (f) potential temperature (θ) and silicate at the station north of the equator (7°30'N, 46°40'W) during the CITHER 1 cruise.

27.25 isopycnal, as also observed by *Bub and Brown* [1996] in the western tropical Atlantic. This density level lies between that (σ_θ = 27.20) chosen generally to describe the AAIW features south of 20-25°S [*Reid*, 1989; *Warner and Weiss*, 1992; *Tsuchiya et al.*, 1994], and that (σ_θ = 27.30) used by *Suga and Talley* [1995] in the subequatorial gyre. The decline in the prominence of the oxygen maximum north of the equator (Figure 2e) would thus be due to the mixing of AAIW, as it crosses the equator, with the strong oxygen minimum of the equatorial zone [*Reid*, 1989]. The slight bulges in the CFC profiles (Figures 2b and 2e) at around 600-700 dbar are clearly related to the oxygen maximum. This feature is indicative of the recent ventilation of AAIW and agrees with similar conclusions drawn by *Warner and Weiss* [1992], who traced the spreading of AAIW as far as the equator, and by *Roether and Putzka* [1996], within the South Atlantic, using this transient tracer.

3.3. Identification of UCPW Near the Equator

Tschuiya et al. [1994] assign a density of σ_θ = 27.40 to UCPW north of 20°S, the same as the density of circumpolar water at the sea surface in winter [*Reid*, 1989]. At the southern edge of the equatorial belt (near 5°S) this density layer lies beneath the AAIW layer and near the 1000-dbar level. Both south and north of the equator, the temperature minimum and silicate maximum, characteristic of the UCPW, also become clearly distinct (about 200-300 dbar deeper) from the salinity minimum and dissolved oxygen maximum that characterize the AAIW (Figure 2). The phosphate (Figures 2a and 2d) and nitrate (not shown) maxima were also located exactly at the depth of the silicate maximum on the western boundary [see also *Oudot et al.*, 1998].

The lowest CFC concentrations (< 0.02 pmol kg^{-1}) near the core of the UCPW (Figure 2) indicate the poor ventilation of an old water mass, in contrast with the recently ventilated overlying AAIW and underlying UNADW [*Andrié et al.*, 1998]. The striking feature in the CFC-11 profile in the southern transect is the coincidence of the CFC minimum with the lower oxygen minimum layer, both of which lie at a slightly deeper (about 200 dbar) and denser (σ_θ = 27.55) layer than the silicate and temperature extremes (σ_θ = 27.40) (Figures 2b and 2c). North of the equator, the CFC minimum and the temperature-silicate extremes lie at the same depth and density layer (1000 dbar and 27.40 σ_θ) (Figures 2e and 2f). This northward shoaling corresponds to the erosion downstream of the UCPW minimum by the underlying CFC-rich UNADW flowing from the north [*Andrié et al.*, 1998]. The same feature, erosion of the CFC minimum of the UCPW and its shoaling toward north, has also been recognized farther south in the Atlantic [*Roether and Putzka*, 1996]. A combination of geochemical (nutrients) and transient (CFC) tracers thus enable a clear differentiation of AAIW and UCPW in the equatorial Atlantic, in spite of the proximity of their levels and poor vertical extension.

4. AAIW Circulation

Circulation of AAIW in the western equatorial Atlantic was examined on the σ_θ = 27.25 isopycnal. Within the western Atlantic delimited by the two CITHER1 transects and the 35°W section, this density layer lies at a mean depth of 676 ±36 dbar. In the northwestern tropical Atlantic, *Bub and Brown* [1996] locate this density layer at approximately 700 m.

4.1. AAIW Arrival Along the Western Boundary

The low-salinity (< 34.4) and high-oxygen content (> 195 µmol kg^{-1}, i.e., 4.4 mL L^{-1}) [*Arhan et al.*, 1998], accompanied by high CFC concentrations (CFC-11 > 0.3 pmol kg^{-1}) and a pronounced nutrient minimum (phosphate < 2.1 µmol kg^{-1} and nitrate < 30 µmol kg^{-1}) [*Oudot et al.*, 1998] in the southern CITHER 1 transect (Figure 3), herald the entry of AAIW on the western boundary of the equatorial belt [see also *Schott et al.*, 1995]. The similarity between the tracer (salinity, oxygen, phosphate, and CFC) concentrations at the westernmost stations of the 5°S section and the southernmost stations of the 35°W section (Figure 3) clearly shows the westward continuity of AAIW along the northern coast of Brazil as a narrow flow (< 100 km from the coast) during CITHER 1 (January-February 1993). The distribution of the tracers along the 5°S section (Figures 3b and 3c) also shows another narrow northward flow, with eroded AAIW characteristics, at about 220 km offshore (33°W). The reversal of the σ_θ = 27.25 isopycnal slope between 100 and 300 km (Figure 3a) suggests a southward flow between these two northward flows.

Along 35°W the tracer concentrations change progressively but not monotonously, toward the north and less rapidly than at 5°S at equal distances from the coast (Figure 3). The tracer extremes (minima of salinity/phosphate and maxima of oxygen/CFC) at about 2°30'S (250 km offshore) along the 35°W section signify an eastward recirculation flow of AAIW (see Figure 5) that enters the western equatorial basin as a coastal flow along Brazil. The northward deepening of the σ_θ = 27.25 isopycnal between 100 and 300 km along 35°W also confirms the presence of an eastward AAIW flow. It is unlikely that the tracer extremes at 35°W, 2°30'S represent a westward extension of the offshore AAIW flow at 5°S and 33°W, since the oxygen-CFC concentrations here are higher and widespread than at 5°S, 33°W. Consequently, the offshore branch of northward AAIW flow observed at 5°S, 33°W would rather turn eastward downstream and join the eastward AAIW flow identified along 35°W in a southern equatorial branch, as suggested earlier by the circulation map of *Reid* [1989] at 800 dbar and described farther eastward (25°W) by *Suga and Talley* [1995].

4.2. Variability of AAIW Circulation Pathways

The spreading of AAIW in the western equatorial region was traced using the S-O_2 relationship, supported by ADCP current measurements when available and vertical oscillations of the isopycnal surface, indicative of the geostrophic flow directions, when the latter are not available. Following the water mass analysis of *Wilson et al.* [1994], a S-O_2 diagram, combining data on the σ_θ = 27.25 isopycnal from all stations in the three cruises (Figure 4), was constructed. This was done to show that, irrespective of the cruise, the S-O_2 characteristics on this isopycnal lie roughly along a line connecting two points representing the extreme S-O_2 characteristics encountered at the boundaries of the study area. The end-member A corresponds to the lowest salinity (34.38) and highest oxygen content (195 µmol kg^{-1}) characteristics of AAIW transported by the lower part of the

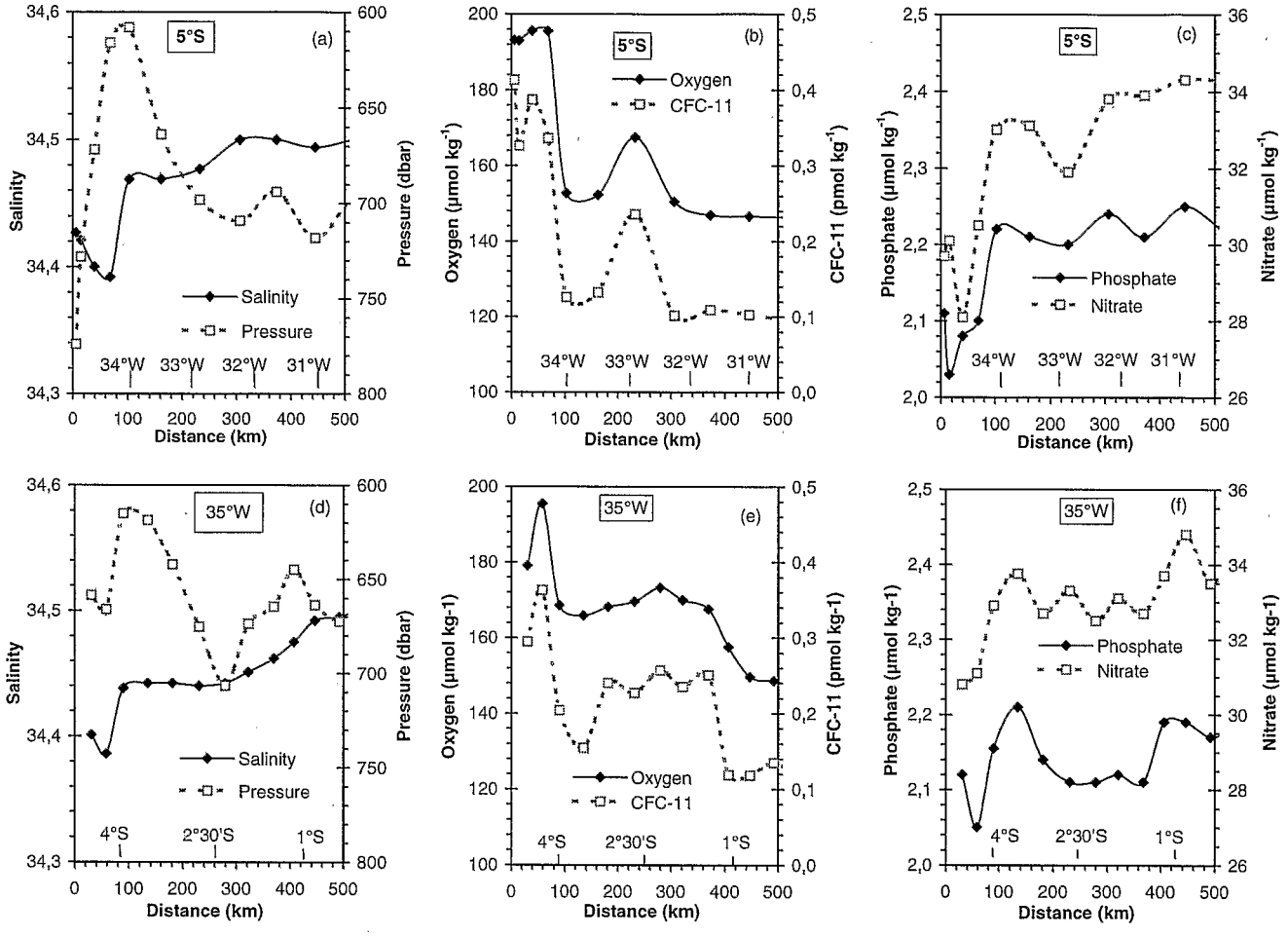

Figure 3. Distribution on isopycnal σ_θ = 27.25 of (a) salinity and pressure, (b) oxygen and CFC-11, and (c) phosphate and nitrate along 5°S and (d) salinity and pressure, (e) oxygen and CFC-11, and (f) phosphate and nitrate along 35°W during the CITHER 1 cruise. The distance (km) is indicated from the shelf break off Brazil.

North Brazil Undercurrent (NBUC) near Cape San Roque (Figures 3d and 3e). The end-member B corresponds to the highest-salinity (34.73) and lowest-oxygen content (93 µmol kg^{-1}) of the overlying strong oxygen minimum that originates in the eastern equatorial Atlantic. This minimum is advected westward across 35°W by the deep equatorial edges of the South and North Equatorial Currents and becomes evident at the northeast corner (7°30'N, 35°W; see *Arhan et al.* [1998, Figures 5 and 9]). The intermediate water on 27.25 σ_θ is thus considered to have resulted from a mixing process between these two end-members. The large scatter of points during ETAMBOT 1 is due to the poor vertical resolution of sampling between 500 and 1000 dbar in that cruise and the consequent uncertainties in the interpolation on the isopycnal surface.

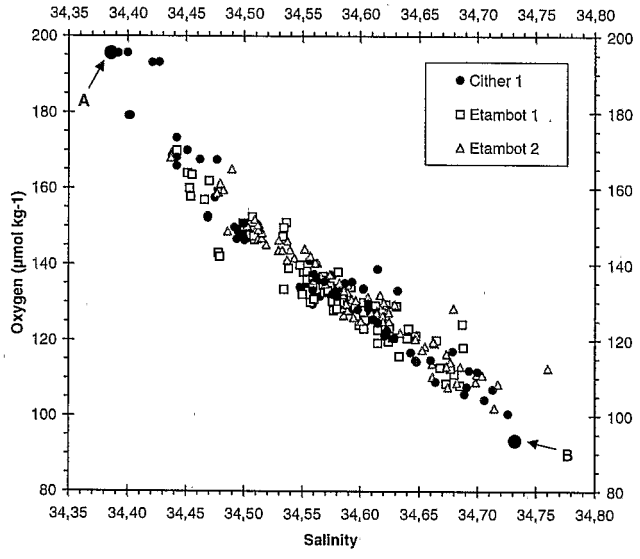

Figure 4. Salinity-oxygen diagram on isopycnal σ_θ = 27.25 from data in all three cruises. A and B refer to the two end-member water masses at their points of entry in the study area. Core tracer values are 34.38 and 195 µmol kg^{-1} for southern water and 34.73 and 93 µmol kg^{-1} for eastern equatorial water.

Figures 5-7 (left) show the percentage of A (southern intermediate water) extracted from the binary mixing and the ADCP (SADCP for CITHER 1 and LADCP for ETAMBOT) velocities (positive eastward component along 35°W and Ceara and positive northward component along 7°30'N). The pressure variations of the isopycnal surface are shown in Figures 5-7 (right) to indicate the geostrophic flow direction. The maximum ADCP velocities (positive eastward/northward and negative

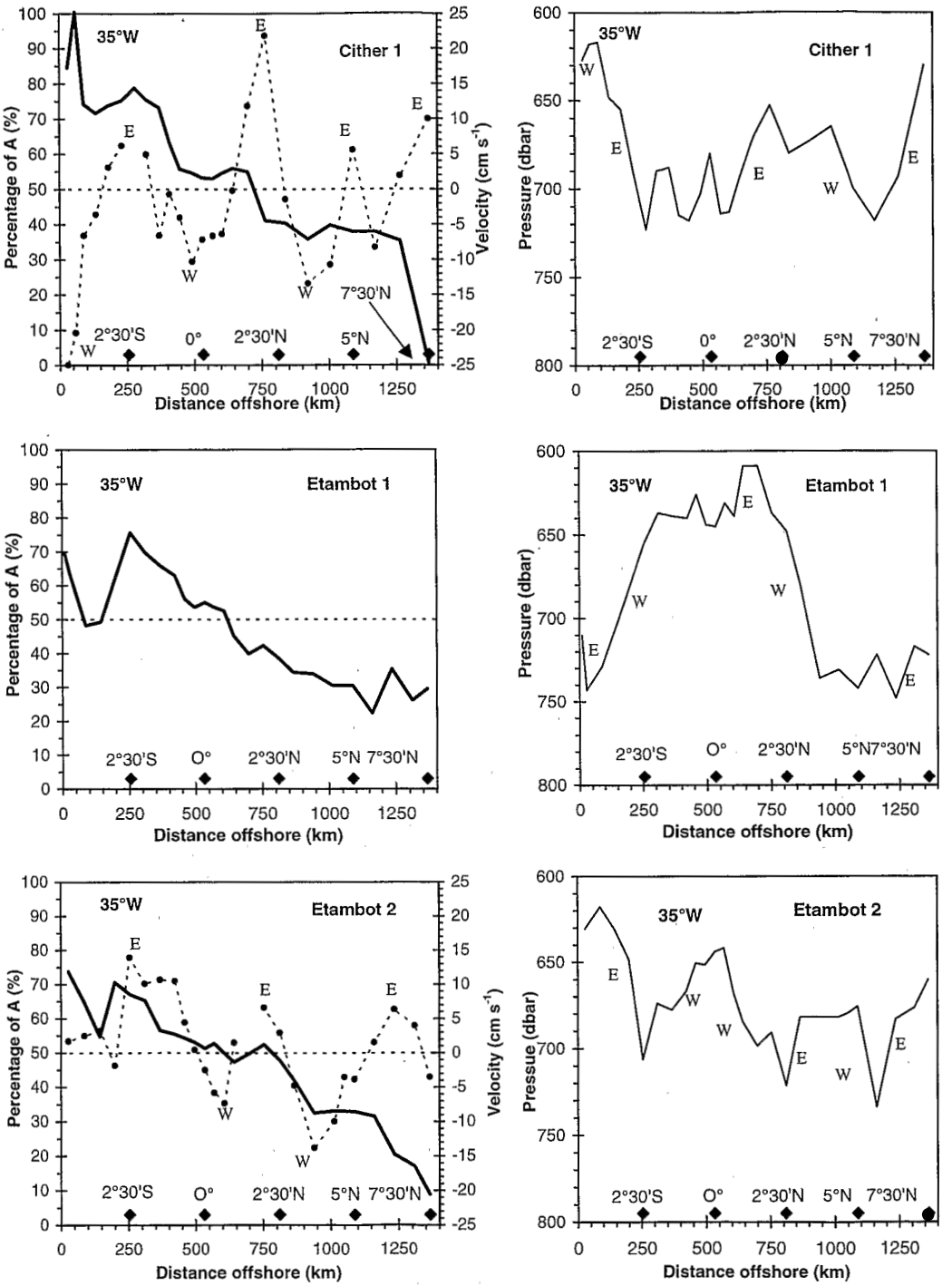

Figure 5. (left) Distribution of the percentage of the southern water (fraction of A) and acoustic Doppler current profiler (ADCP) velocity on the isopycnal $\sigma_\theta = 27.25$ along the 35°W section in the three cruises. Positive values indicate eastward velocities, and negative values indicate the westward velocities. (right) Distribution of the pressure of the isopycnal $\sigma_\theta = 27.25$ along the 35°W section in the three cruises. South of the equator, southward deepening of the isopycnal corresponds to westward geostrophic currents and the northward deepening to eastward geostrophic currents. North of the equator, northward deepening of the isopycnal corresponds to westward geostrophic currents and the southward deepening corresponds to eastward geostrophic currents.

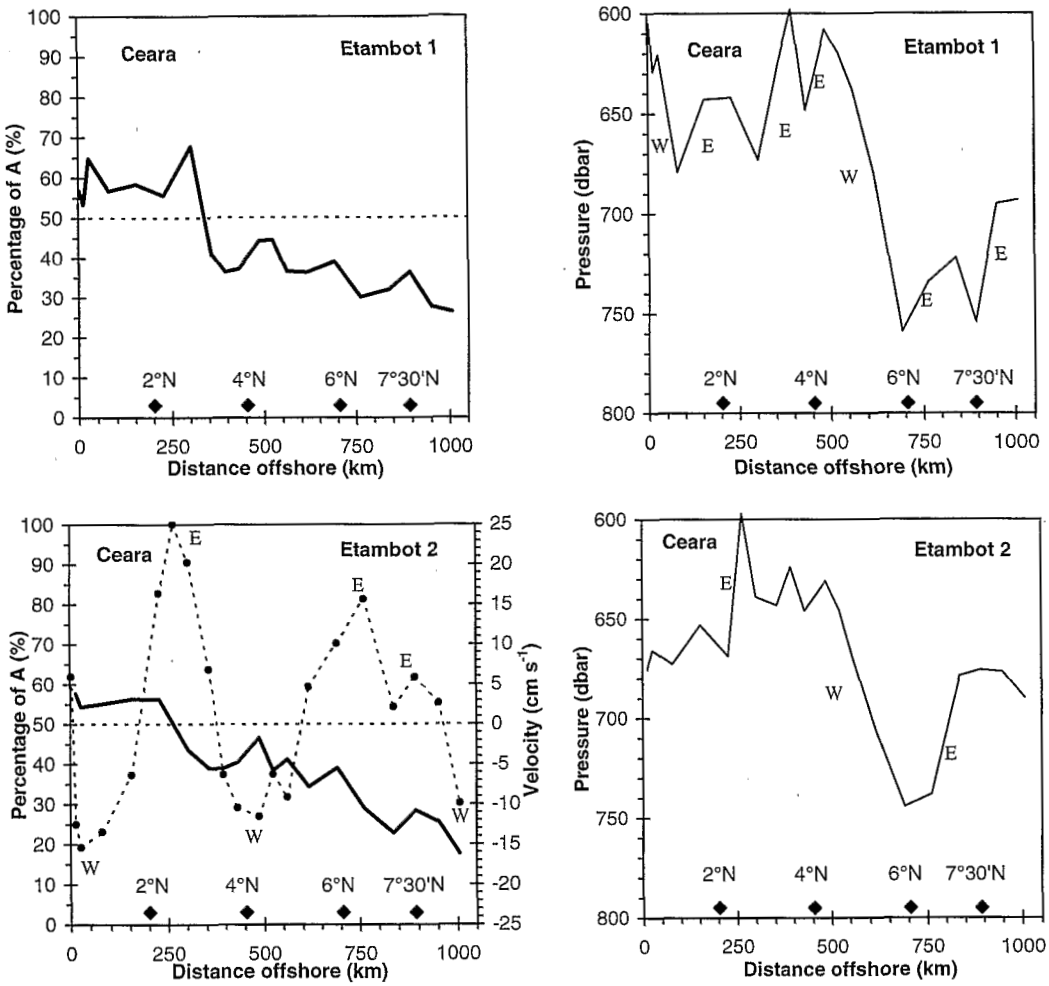

Figure 6. (left) Distribution of the percentage of the southern water (fraction of A) and acoustic Doppler current profiler (ADCP) velocity on the isopycnal $\sigma_\theta = 27.25$, along the Ceara section for the ETAMBOT cruises. Positive values indicate eastward velocities, and negative values indicate westward velocities. (right) Distribution of the pressure of the isopycnal $\sigma_\theta = 27.25$ along the Ceara section during the ETAMBOT cruises. Northward deepening of the isopycnal corresponds to westward geostrophic currents, and southward deepening corresponds to eastward geostrophic currents.

westward/southward) do not always agree with the direction of the flows deduced from the slope of the isopycnal; ADCP velocities are instantaneous current measurements that can be affected by local gyres, whereas the slope of the isopycnal results from an adjustment to the geostrophic flow on a larger scale.

The percentage of A arriving wedged along the Brazilian continental slope region during CITHER 1 was substantially higher, by about 30%, than during both ETAMBOT cruises (Figure 5), obviously related to the high westward velocity measured at that time. During ETAMBOT 1 (summer-fall 1995), the highest A percentage was at 2°30'S, away from the Brazilian coast; the reversal of the isopycnal slope at 2°30'S at this time indicates a westward flow, unlike the eastward flows observed during CITHER 1 and ETAMBOT 2, which were undertaken in winter-spring. The northward decline in the percentage of A along 35°W is not continuous but is interrupted at 250 km (around 2°30'S), 650-750 km (1-2°N), and 1100-1200 km (6-7°N), indicating eastward recirculation limbs. The bulges are more pronounced during CITHER 1 and ETAMBOT 2 than during ETAMBOT 1, suggesting that the eastward recirculations are less vigorous during the latter period; nevertheless, at 7°30'N, the percentage of A is clearly higher during ETAMBOT 1 than during CITHER 1 and ETAMBOT 2. Besides these, a feature that is remarkable in the distribution of the percentage of A is its intercruise stability (50 to 55%) within the westward flow at the equator (Figure 5), called the Equatorial Intermediate Current (EIC) at that depth [*Schott et al.*, 1995, 1998; *Gouriou et al.*, this issue], in contrast with the seasonal variability of the EIC transport, minimum in June and maximum in November, observed by *Schott et al.* (1998).

The LADCP measurements (ETAMBOT 2) and the poleward deepening of the 27.25 σ_θ surface (ETAMBOT 1) in the Ceara section (Figure 6) show that the coastal flow is westward. A comparison of the percentage of A between the two ETAMBOT cruises (Figure 6) shows that it is higher (> 60%) and more spread out (over 300 km) at the southern edge during ETAMBOT 1 than during ETAMBOT 2 (only 55% and 200 km). This westward extension of more southern water during ETAMBOT 1 is related to a diminished eastward recirculation north of the equator along 35°W (see above). Farther north, other

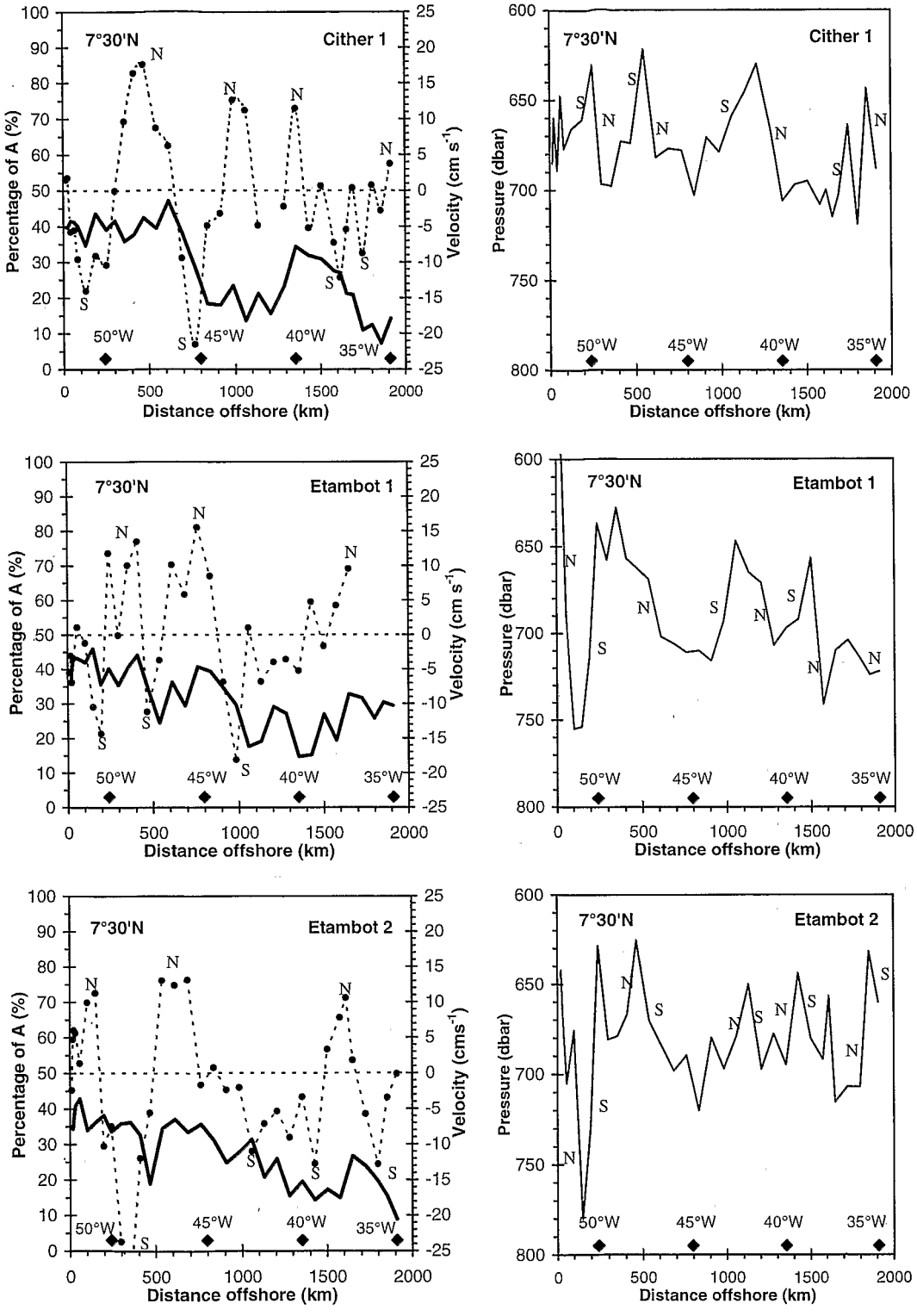

Figure 7. (left) Distribution of the percentage of the southern water (fraction of A) and acoustic Doppler current profiler (ADCP) velocity on the isopycnal $\sigma_\theta = 27.25$, along the 7°30'N section in the three cruises. Positive values indicate northward velocities, and negative values indicate southward velocities. (right) Distribution of the pressure of the isopycnal $\sigma_\theta = 27.25$ along the 7°30'N section in the three cruises. Eastward deepening of the isopycnal corresponds to northward geostrophic currents, and westward deepening corresponds to southward geostrophic currents.

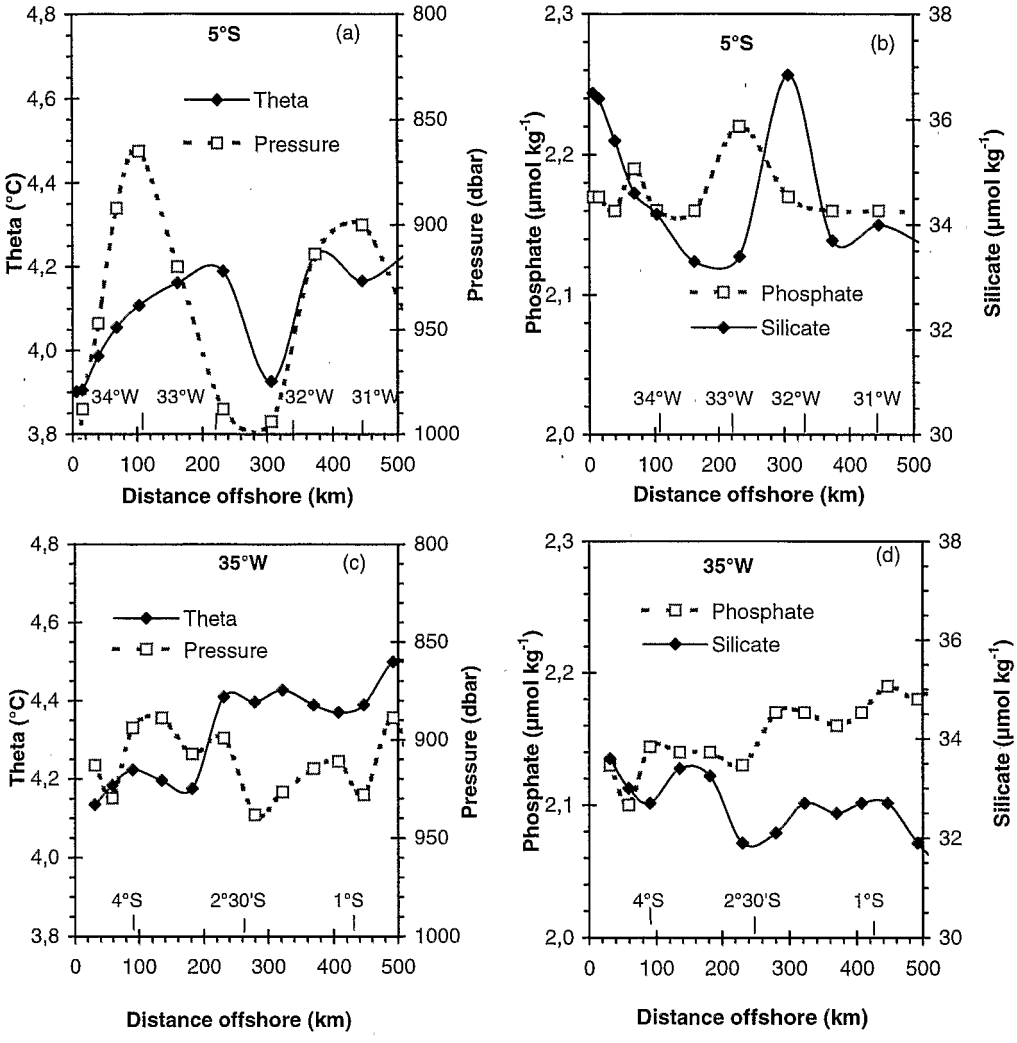

Figure 8. Distribution on isopycnal $\sigma_\theta = 27.40$ of (a) potential temperature (θ) and pressure, (b) phosphate and silicate along 5°S and (c) potential temperature (θ) and pressure, (d) phosphate and silicate along 35°W during the CITHER 1 cruise.

discontinuities during both ETAMBOT cruises in the decline of the percentage of A (4°N, 6°N and 7°30'N) represent, consistent with the LADCP measurements or vertical oscillations of the isopycnal $\sigma_\theta = 27.25$, eastward recirculations. The front just north of 2°N is associated with an eastward flow on its south side, which can be seen more clearly during ETAMBOT 2.

Farther north and west, the percentage of A becomes highly variable along the 7°30'N section (Figure 7), but, in general, tends to decrease away from the coast. Nevertheless, the highest percentage of A (>45%) in the CITHER 1 section was not inshore but at 600 km, which would probably explain why *Arhan et al.* [1998] did not identify any trace of a boundary current at the AAIW level. On the other hand, during ETAMBOT 1, the percentage of A tended to increase on the eastern edge (east of 40°W). Maximum percentages of A were generally associated with northward flows and the minimum, with southward flows, as measured with the acoustic current profiler (SADCP during the CITHER 1 cruise and LADCP during both ETAMBOT cruises) (Figure 7, left).

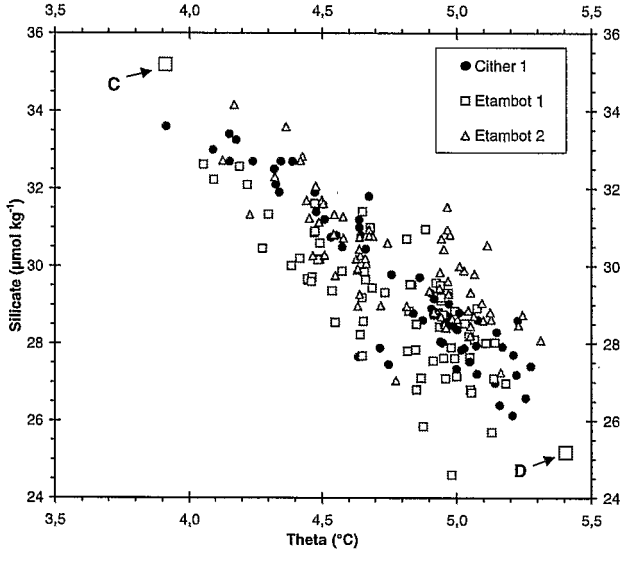

Figure 9. Potential temperature-silicate diagram on isopycnal $\sigma_\theta = 27.40$ from data in the three cruises. C and D refer to the two end-member water masses at their points of entry in the study area. Core tracer values are 3.9 °C and 35.2 µmol kg^{-1} for southern water and 5.4 °C and 25.2 µmol kg^{-1} for northern water.

5. UCPW Circulation

Apart from the CFC minimum, the temperature minimum and silica maximum are the visible signatures of the UCPW flow (see above), both of which can be clearly seen on the σ_θ = 27.40 isopycnal (Figures 2c and 2f). Hence this density surface was chosen to examine UCPW circulation. In the western equatorial belt this surface lies at 919 ±35 dbar, about 240 dbar deeper than that of AAIW (676 ±36 dbar). This depth interval is slightly lower than that (300 m) between the temperature minimum of the UCPW and the salinity minimum of the AAIW, as also has been shown farther south [*Tsuchiya et al.*, 1994].

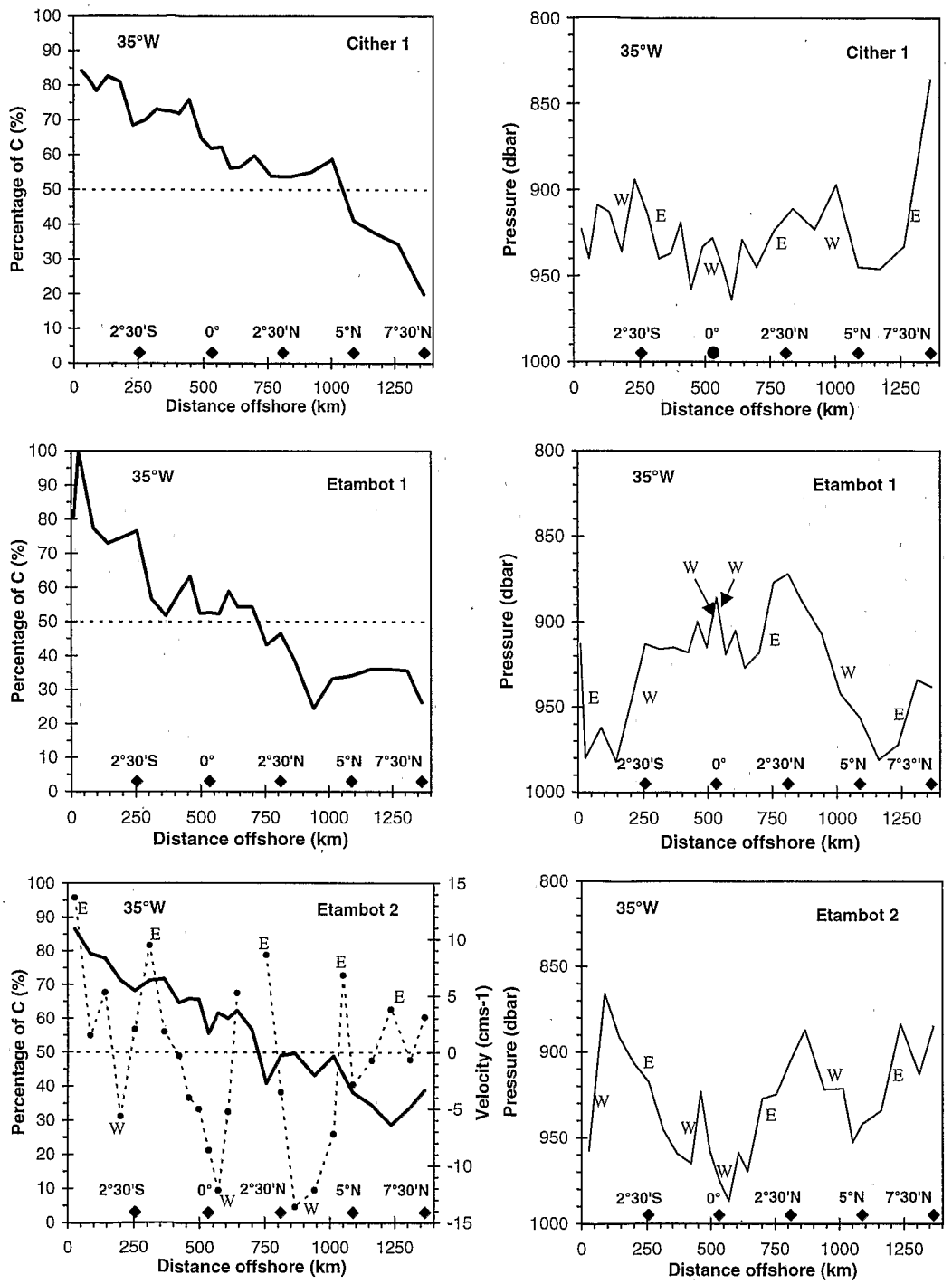

Figure 10. (left) Distribution of the percentage of the southern water (fraction of C) and acoustic Doppler current profiler (ADCP) velocity on the isopycnal σ_θ = 27.40, along the 35°W section in the three cruises. Positive values indicate eastward velocities, and negative values indicate westward velocities. (right) Distribution of the pressure of the isopycnal σ_θ = 27.40 along the 35°W section in the three cruises. South of the equator, southward deepening of the isopycnal corresponds to westward geostrophic currents and the northward deepening corresponds to eastward geostrophic currents. North of the equator, northward deepening of the isopycnal corresponds to westward geostrophic currents and the southward deepening corresponds to eastward geostrophic currents.

5.1. UCPW Arrival Along the Western Boundary

The distribution of temperature and silicate on the 27.40 σ_θ surface along 5°S (Figures 8a and 8b) show that UCPW, like AAIW, enters the equatorial belt as a narrow, northward flow (see the westward deepening of the isopycnal, Figure 8a) wedged around the eastern tip of Brazil and as another northward flow at 300 km offshore (about 32°W) [*Arhan et al.*, 1998; *Oudot et al.*, 1998]. However, several differences in the tracer properties and their changes between UCPW and AAIW can be seen. In the first instance the offshore northward flow of UCPW retains the temperature and silicate signatures as clearly as in the coastal flow, whereas that of the AAIW has substantially eroded core properties. In the second the increase in temperature from < 3.9°C to > 4.1°C and decrease in silicate from > 36 µmol kg^{-1} to < 34 µmol kg^{-1} (Figures 8c and 8d), however, show that the core properties of UCPW, unlike AAIW, are heavily eroded during its transit between the western end of the 5°S section and the southern end of the 35°W section. In the last, again unlike AAIW, the oxygen and CFC concentrations on the σ_θ = 27.40 surface do not show clear changes along the coast, except for a small downstream increase in CFC-11 (not shown here), owing to the mixing with the overlying (AAIW) and underlying (UNADW) CFC-enriched layers.

5.2. Variability of UCPW Circulation Pathways

The flow pathways of UCPW were traced using a temperature-silicate mixing diagram (Figure 9), as was done with the oxygen-salinity diagram for AAIW. The end-member C denotes the southern water issued from the UCPW (temperature, 3.9°C; silicate, 35.2 µmol kg^{-1}), and the end-member D denotes the northern water derived from NADW (temperature, 5.4°C; silicate, 25.2 µmol kg^{-1}). The tracer concentrations of the end-member waters were selected from the ETAMBOT 1 data.

Figures 10-12 show the percentage of the southern water C extracted from the mixing diagram, along with the flow direction, indicated by LADCP velocity (positive eastward component along 35°W and Ceara and positive northward along 7°30'N) and

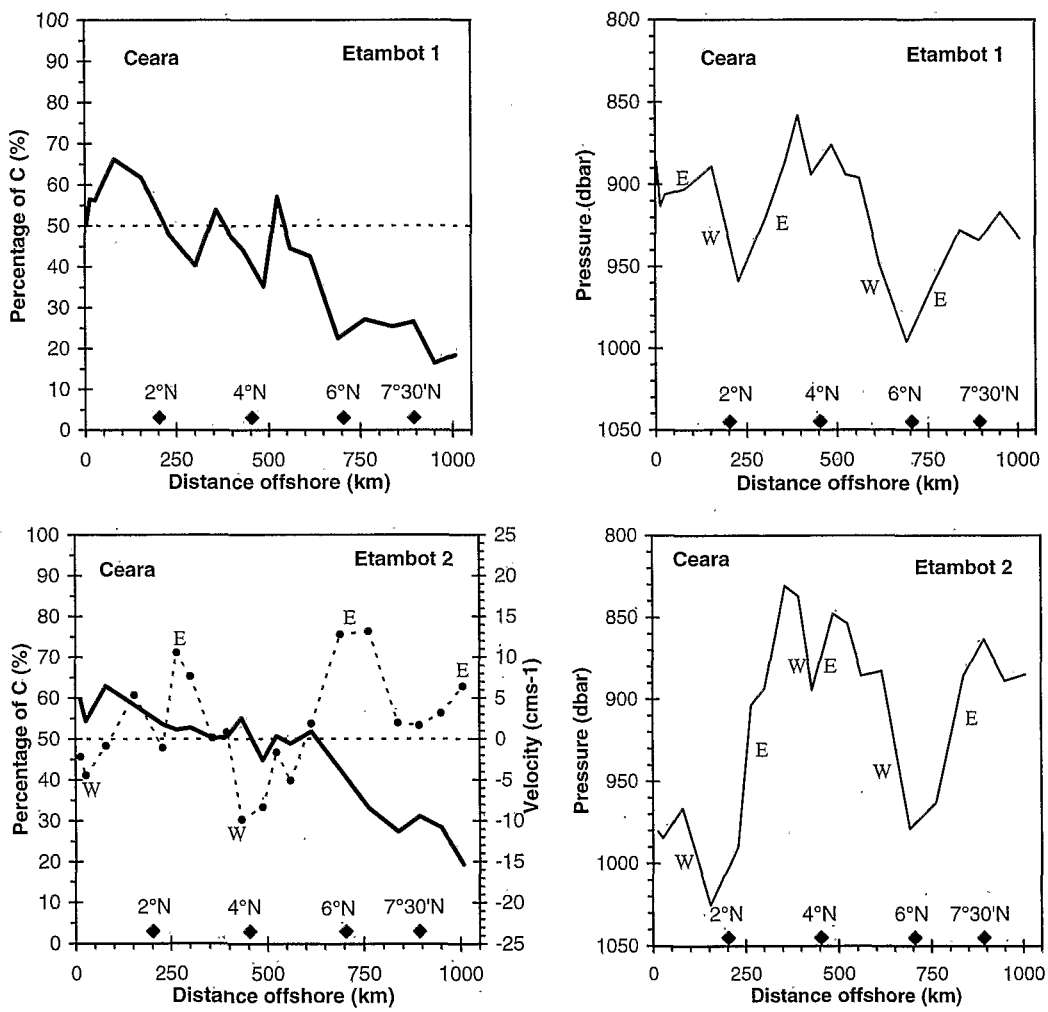

Figure 11. (left) Distribution of the percentage of the southern water (fraction of C) and acoustic Doppler current profiler (ADCP) velocity on the isopycnal σ_θ = 27.40, along the Ceara section for the ETAMBOT cruises. Positive values indicate eastward velocities, and negative values indicate westward velocities. (right) Distribution of the pressure of the isopycnal σ_θ = 27.40 along the Ceara section during the ETAMBOT cruises. Northward deepening of the isopycnal corresponds to westward geostrophic currents and southward deepening corresponds to eastward geostrophic currents.

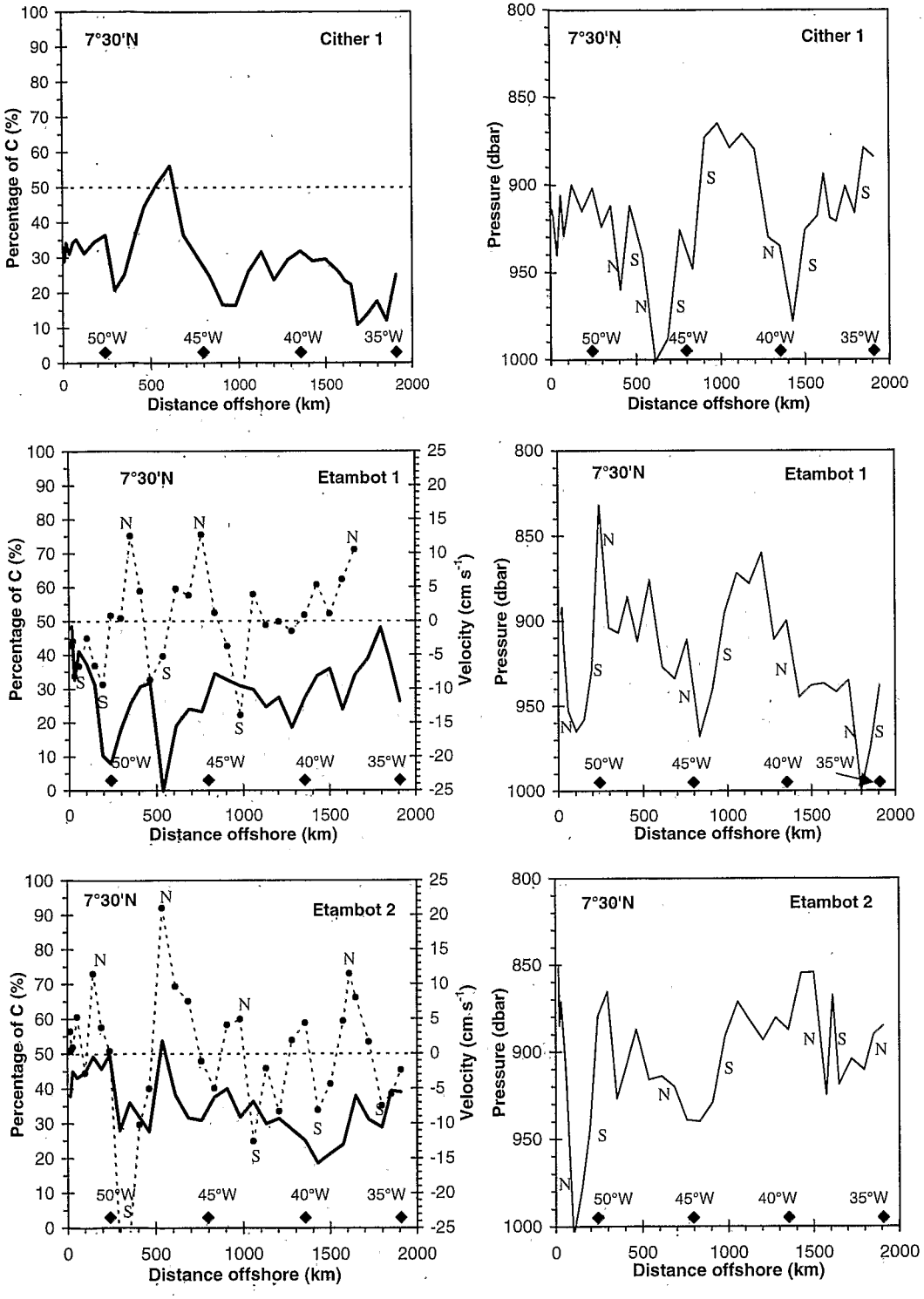

Figure 12. (left) Distribution of the percentage of the southern water (fraction of C) and acoustic Doppler current profiler (ADCP) velocity on the isopycnal $\sigma_\theta = 27.40$, along the 7°30'N section in the three cruises. Positive values indicate northward velocities, and negative values indicate southward velocities. (right) Distribution of the pressure of the isopycnal $\sigma_\theta = 27.40$ along the 7°30'N section in the three cruises. Eastward deepening of the isopycnal corresponds to northward geostrophic currents and westward deepening corresponds to southward geostrophic currents.

the pressure of 27.40 σ_θ surface. The northward decrease in the percentage of C along the 35°W section (Figure 10) is not smooth but is punctuated with bulges that are generated by alternative westward and eastward components of the zonal flow. These were deduced from the topography of the σ_θ = 27.40 isopycnal (Figure 10, right) or from the LADCP measurements during ETAMBOT 2 (Figure 10, bottom left). As was the case with the AAIW (Figure 5), the largest anomalies were in the CITHER 1 section. Taking the >50% of C as indicative of a predominance of the southern water, the spread of the latter during ETAMBOT 1, except for a high percentage observed at 50 km offshore, is less (<750 km) compared with that (>1000 km) during CITHER 1 and ETAMBOT 2 (Figure 10). Using this same index, it can be seen that the southern water spreads farther offshore also along the Ceara section (Figure 11) during ETAMBOT 2 than during ETAMBOT 1, indicating a certain continuity of the circulation pattern over this longitudinal range (35°W – 45°W). Nevertheless, on the 27.40 σ_θ, the association of anomalies of the southern water fraction with eastward recirculations (see LADCP velocity during ETAMBOT 2) is not as regular as it was on the 27.25 σ_θ.

The interesting feature along the 7°30'N section is that the variability of the percentage of C between the three cruise periods (Figure 12) is substantially high, compared with that of A on σ_θ = 27.25 (Figure 7). The highest percentage of southern water (>50%) on the UCPW density level occurs far from the continental shelf, beyond 500 km during CITHER 1 and ETAMBOT 2 and as far away as 1800 km offshore during ETAMBOT 1, with no clear trend of decrease with distance offshore, as was seen on the AAIW density surface; in fact, the percentage of C during ETAMBOT 1 appears to increase offshore east of 50°W. In most cases, maximum values of the C percentage are associated with northward flows, as indicated by eastward deepening of the 27.40 σ_θ isopycnal or positive LADCP velocity, and the minimum values are associated with the southward flows.

6. Discussion and Summary

Although the AAIW and UCPW lie close to each other, the depth interval between these two water masses is still significant and is comparable with the vertical scale of the velocity structure of the deep equatorial currents (200-300 m) within the same depth range (500-1000 m) [*Gouriou et al.*, this issue]; it is therefore not surprising to find significant differences in the circulation patterns between them. In fact, the high-resolution circulation model of *Böning and Schott* [1993] predicts zonal currents above and below 700-900 m depth, flowing in opposite directions and changing their directions seasonally. While our results generally conform with these predictions, their quantitative extents are constrained by uncertainties in the definition of core tracer values of representative end-member water masses. The chosen end-members are neither pure water types nor can their tracer concentrations be expected to be invariant over time; a ±1 μmol kg^{-1} uncertainty in silicate or a ±6 μmol kg^{-1} difference in dissolved oxygen content, for instance, can produce ±5 % variation in the proportion of southern water at any one point. The dispersion of points around the mixing line, especially on σ_θ = 27.40, does, in fact, suggest a certain degree of interference from other water masses and diapycnal mixing. Nevertheless, this approach, combining hydrographic (temperature, salinity) and geochemical tracers (oxygen, silicate), is still useful in identifying the prominent pathways of water masses of southern origin at these density levels.

Both AAIW and UCPW enter the western equatorial basin as narrow northwestward flows (<100 km) wedged against the continental slope around Cape San Roque (eastern Brazil). Farther away from Cape San Roque, the characteristics of UCPW become more eroded than those of AAIW, indicating a larger mixing of the former with surrounding waters. Two other narrow, northward flows along 5°S off the continental shelf, one at 220 km (33°W) from the continent on the AAIW level and another at 300 km (32°W) on the UCPW level, also become evident. The steeper slope of the σ_θ = 27.40 isopycnal (eastward deepening between 34°W and 32°W), compared with that of σ_θ = 27.25 (from 34°W to 33°W) (Figures 3a and 8a), suggests a stronger southward flow, probably related to the underlying southward flow of NADW, that could shift the northward offshore branch of UCPW farther away from the continent. Our results show that, at both levels, the northward offshore branch does not flow continuously westward but appears, rather, to have eastward deviations, conforming with the flow pattern proposed by *Reid* [1989] at 800 dbar on the western boundary just south of the equator. At 35°W the main westward flow of AAIW is relatively far away from the continental slope (about 200 km), particularly in late summer 1995 (ETAMBOT 1) (Figure 5), whereas that of UCPW remains, in each cruise, closer to the coast (Figure 10). Moreover, the prominent signatures of AAIW and UCPW reaching 35°W do not appear during the same cruise: the AAIW signatures were prominent during CITHER 1, and those of UCPW were prominent during ETAMBOT 1.

The strength and pathway of AAIW flow spreading northwestward beyond the Cape San Roque undergo seasonal changes. The discontinuities in the meridional decrease of the percentage of southern water A on 27.25 σ_θ away from the coast along 35°W are more pronounced during CITHER 1 (winter) and ETAMBOT 2 (spring) than during ETAMBOT 1 (late summer) (Figure 5), suggesting that eastward recirculations on both sides of the equator (as far as 5°N) are more prominent during the former periods. However, the percentage of A was higher farther westward (45°W), indicating a wider spread along the southern edge of the Ceara section, and also northward (6°N) at 35°W during ETAMBOT 1 than during ETAMBOT 2 and CITHER 1. These variations suggest that the eastward recirculation of southern water occurs farther westward (through the Ceara section) and then northward (north of 5°N at 35°W) during ETAMBOT 1 (late summer) than during the other two cruises (winter and spring). This finding is consistent with the seasonal variability shown previously east of 44°W [*Schott et al.*, 1993, 1998; *Stramma and Schott*, 1996) and that deduced for the NECC [*Richardson and Reverdin*, 1987; *Richardson et al*, 1992] in upper layers, according to which, the NECC in summer is mainly fed by southern water through the NBC retroflection. Such a seasonal variation is not as pronounced at the UCPW level (Figures 10 and 11).

The distributions of the A and C percentages of the southern component water along the 7°30'N section show that the pathways of AAIW and UCPW north of the equatorial belt are quite different. Regardless of the season, the percentage of AAIW-derived water decreases significantly from the coast to the east along this section (Figure 7), while that of UCPW-derived water, though highly variable within a season, remains high at the eastern extremity, near 35°W (Figure 12). At this latitude the

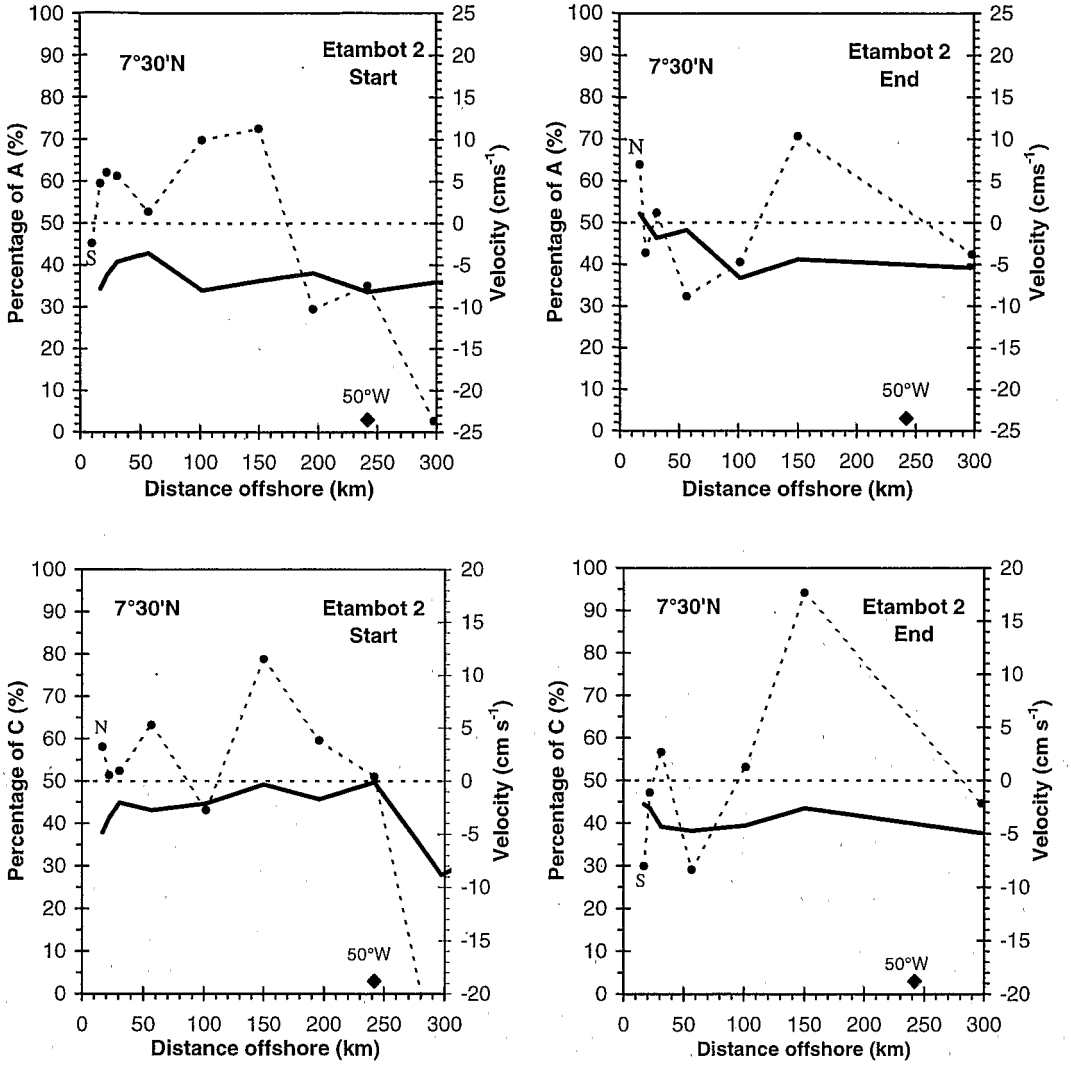

Figure 13. Distributions of the percentages of the southern waters (fraction of A and C) and acoustic Doppler current profiler (ADCP) velocity in the water layer on isopycnal (top) σ_θ = 27.25 and (bottom) σ_θ = 27.40 off French Guiana along the 7°30'N section at the beginning and end of the ETAMBOT 2 cruise. Positive values indicate northward velocities, and negative values indicate southward velocities.

AAIW-derived water flows along the western boundary while the UCPW-derived water spreads, instead, toward the interior of the ocean. Besides this, short-term variations in the fraction of the water of southern origin, of the order of a month, could also occur at the AAIW level than at the UCPW level. For example, in the 30-day period between the start and the end of the ETAMBOT 2 cruise, the percentage of southern water on the σ_θ = 27.25 level off French Guyana increased, concurrent with the reversal of the westernmost flow, from 35% to >50% (Figure 13). However, within the same period, the percentage of C at σ_θ = 27.40 remained more or less constant (40% ± 5%) (Figure 13), even though there was also a reversal of currents at this density level but in a direction opposite of that in the AAIW layer (Figure 13). This observation suggests that short-term variability is confined to the coastal flow, but as repeat observations were made only during ETAMBOT 2, it would be difficult to state whether this also occurs in other seasons.

Our observations thus confirm that the northward paths of the AAIW and UCPW carried by the NBUC around the corner of the South American continent are complex, with their spreading modes within the western equatorial domain punctuated by eastward recirculations of the NBC that change with time and depth.

Acknowledgments. We are grateful to B. Bourlès and Y. Gouriou (IRD, Brest) for ADCP current data and help in processing a number of figures. Financial support for the cruises was provided by the Institut de Recherches pour le Développement (IRD) (previously Office de la Recherche Scientifique pour le Développement en Coopération (ORSTOM)), Institut Français pour l'Exploitation de la Mer (IFREMER), and Institut National des Sciences de l'Univers (INSU), under the French Programme National d'Etude de la Dynamique du Climat (PNEDC), a contribution to WOCE.

References

Andrié, C., J.F. Ternon, M.J. Messias, L. Memery, and B. Bourlès, Chlorofluoromethanes distributions in the deep equatorial Atlantic during January-March 1993, *Deep Sea Res. Part I, 45*, 903-930, 1998.

André, C., J.F. Ternon, B. Bourlès, Y. Gouriou, and C. Oudot, Tracer distributions and deep circulation in the western tropical Atlantic during CITHER 1 and ETAMBOT cruises (1993-1996), *J. Geophys. Res.*, this issue.

Arhan, M., H. Mercier, B. Bourles, and Y. Gouriou, Two hydrographic sections across the Atlantic at 7°30N and 4°30S, *Deep Sea Res., Part I, 45*, 829-872, 1998.

Boebel, O., C. Schmid, and W. Zenk, Flow and recirculation of Antarctic Intermediate Water across the Rio Grande Rise, *J. Geophys. Res., 102* 20,967-20,986, 1997.

Böning, C. W., and F. A. Schott, Deep currents and eastward salinity tongue in the equatorial Atlantic: Results from an eddy resolving, primitive equation model, *J. Geophys. Res., 98*, 6991-6999, 1993.

Bourlès, B., R.L. Molinari, E. Johns, W.D. Wilson, and K.D. Leaman, Upper layer currents in the Western Tropical North Atlantic (1989-1991), *J. Geophys. Res., 104*, 1361-1375, 1999.

Bourlès B., Y. Gouriou, and R. Chuchla, On the circulation in the upper layer of the western equatorial Atlantic, *J. Geophys. Res.*, this issue.

Brown, W.S., W.E. Johns, K.D. Leaman, J.P. McCreary, R.L. Molinari, P.L. Richardson, and C. Rooth, A Western Tropical Atlantic Experiment (WESTRAX), *Oceanography, 5*, 73-77, 1992.

Bub, F. L., and W. S. Brown, Intermediate layer water masses in the western tropical Atlantic Ocean, *J. Geophys. Res., 101*, 11.903-11.922, 1996.

Chuchla, R., B. Bourlès, and Y. Gouriou, Mesures de courant avec le profileur à effet Doppler 'profond' (L-ADCP), in Recueil de Données, Campagne ETAMBOT 1, vol. 1, Introduction-Mesures 'en route'-Courantométrie ADCP-Mesures $CTDO_2$-Coupes de distributions verticales, *Doc. Sci. 22*, pp. 87-123, Cent. ORSTOM, Cayenne, French Guiana, 1997a.

Chuchla, R., B. Bourlès, and Y. Gouriou, Mesures de courant avec le profileur à effet Doppler 'profond' (L-ADCP), in Recueil de Données, Campagne ETAMBOT 2, vol. 1, Introduction-Mesures 'en route'-Courantométrie ADCP-Mesures $CTDO_2$-Coupes de distributions verticales, *Doc. Sci. 24*, pp. 93-158, Cent. ORSTOM, Cayenne, French Guiana, 1997b.

Didden, N., and F. Schott, Seasonal variations in the western tropical Atlantic: Surface circulation from Geosat altimetry and WOCE model results, *J. Geophys. Res. 97*, 3529-3541, 1992.

Gordon, A.L., Interocean exchange of thermocline water, *J. Geophys. Res.*, 91, 5037-5046, 1986.

Gordon, A.L., R.F. Weiss, W.M. Smethie Jr., and M.J. Warner, Thermocline and intermediate water communication between the South Atlantic and Indian Oceans, *J. Geophys. Res., 97* 7223-7240, 1992.

Gouriou, Y., G. Eldin, and A. Morlière, Mesures de courants avec le profileur Doppler, in Campagne CITHER 1, Recueil de données, vol. 1/4, Mesures "en route"-Courantométrie ADCP et Pegasus, *Doc. Sci. 14*, pp. 59-144, Cent. ORSTOM, Cayenne, French Guiana, 1994.

Gouriou, Y., B. Bourlès, H. Mercier, and R. Chuchla, Deep jets in the equatorial Atlantic Ocean, *J. Geophys. Res.*, this issue.

Larqué, L., K. Maamaatuaiahutapu, and V. Garçon, On the intermediate and deep water flows in the South Atlantic Ocean, *J. Geophys. Res., 102*, 12.425-12.440, 1997.

Maamaatuaiahutapu K., C. Provost, C. André, and X. Vigan, Origin and ages of mode waters in the Brazil-Malvinas Confluence region during austral winter 1994, *J. Geophys. Res.*, this issue.

Mann, C.R., A.R. Coote, and D.M. Garner, The meridional distribution of silicate in the western Atlantic ocean, *Deep Sea Res., 20*, 791-801, 1973.

Metcalf, W. G., Dissolved silicate in the deep North Atlantic, *Deep Sea Res., 16*, suppl., 139-145, 1969.

Oudot, C., and F. Baurand, Mesures des sels nutritifs, in Campagne CITHER 1, Recueil de données, vol. 3/4, Traceurs Géochimiques, 1, *Doc. Sci. 15*, pp.31-66, Cent. ORSTOM, Cayenne, French Guyana, 1994.

Oudot, C., P. Morin, F. Baurand, M. Wafar, and P. Le Corre, Northern and southern water masses in the equatorial Atlantic: Distribution of nutrients in the WOCE A6 and A7 lines, *Deep Sea Res. Part I, 45*, 873-902, 1998.

Reid, J.L., On the total geostrophic circulation of the South Atlantic Ocean: Flow patterns, tracers and transports, *Prog. Oceanogr., 23*, 149-244, 1989.

Reid, J.L., On the total geostrophic circulation of the North Atlantic Ocean: Flow patterns, tracers and transports, *Prog. Oceanogr., 33*, 1-92, 1994.

Richardson, P.L., and G. Reverdin, Seasonal cycle of velocity in the Atlantic North Equatorial Countercurrent as measured by surface drifters, current meters, and ship drifts, *J. Geophys. Res., 92*, 3691-3708, 1987.

Richardson, P.L., and W.J. Schmitz Jr., Deep cross-equatorial flow in the Atlantic measured with SOFAR floats, *J. Geophys. Res., 98*, 8371-8387, 1993.

Richardson, P.L., S. Arnault, S. Garzoli, and J.G. Bruce, Annual cycle of the Atlantic North Equatorial Countercurrents, *Deep Sea Res., Part A, 39*, 997-1014, 1992.

Rintoul, S., South Atlantic interbasin exchange, *J. Geophys. Res., 96*, 2675-2692, 1991.

Roether, W., and A. Putzka, Transient-tracer information on ventilation and transport of South Atlantic waters, in *The South Atlantic: Present and Past Circulation*, edited by G. Wefer et al., pp. 45-62, Springer-Verlag, New York, 1996.

Schmitz, W.J., and P.L. Richardson, On the sources of the Florida Current, *Deep Sea Res., Part A, 38*, supplement, 379-409, 1991.

Schott, F., and C.W. Böning, The WOCE model in the western equatorial Atlantic: Upper layer circulation, *J. Geophys. Res., 96*, 6993-7004, 1991.

Schott, F., J. Fischer, J. Reppin, and U. Send, On mean and seasonal currents and transports at the western boundary of the equatorial Atlantic, *J. Geophys. Res, 98*, 14.353-14.368, 1993.

Schott, F.A., L. Stramma, and J. Fischer, The warm water inflow into the western tropical Atlantic boundary regime, spring 1994, *J. Geophys. Res, 100*, 24745-24760, 1995.

Schott, F.A., J. Fischer, and L. Stramma, Transports and pathways of the upper-layer circulation in the western tropical Atlantic, *J. Phys. Oceanogr., 28*, 1904-1928, 1998.

Stramma, L., and F. Schott, Western equatorial circulation and interhemispheric exchange, in *The Warmwatersphere of the North Atlantic Ocean*, edited by W. Krauss, pp. 195-227, Gebrüder Borntraeger, Berlin, 1996.

Suga, T., and L.D. Talley, Antarctic Intermediate Water circulation in the tropical and subtropical South Atlantic, *J. Geophys. Res, 100*, 13.441-13.453, 1995.

Talley, L. D., Antarctic Intermediate Water in the South Atlantic, in *The South Atlantic: Present and Past Circulation*, edited by G. Wefer et al., pp 219-238, Springer-Verlag, New York, 1996.

Tsuchiya, M., Circulation of the Antarctic Intermediate water in the North Atlantic ocean, *J. Mar. Res., 47*, 747-755, 1989.

Tsuchiya, M., L.D. Talley, and M.S. McCartney, An eastern Atlantic section from Iceland southward across the equator, *Deep Sea Res., Part A, 39*, 1885-1917, 1992.

Tsuchiya, M., L.D. Talley, and M.S. McCartney, Water-mass distributions in the western South Atlantic; A section from South Georgia Island (54S) northward across the equator, *J. Mar. Res., 52*, 55-81, 1994.

Wallace, D.W.R., A. Putzka, and P. Beining, Carbon tetrachloride and chlorofluorocarbons in the South Atlantic Ocean, 19°S, *J. Geophys. Res, 99*, 10.275-10.287, 1994.

Warner, M.J., and R.F. Weiss, Chlorofluoromethanes in South Atlantic Antarctic Intermediate Water, *Deep Sea Res., Part A, 39*, 2053-2075, 1992.

Wilson, W.D., E. Johns, and R.L. Molinari, Upper layer circulation in the western tropical North Atlantic Ocean during August 1989, *J. Geophys. Res., 99*, 22.513-22.523, 1994.

Wüst, G., Schichtung und Zirkulation des Atlantischen Ozeans. Die Stratosphäre, in *Wissenschaftliche Ergebnisse der Deutschen Atlantischen Expedition auf dem Forschungs - und Vermessungsschiff "Meteor"* 1925-1927, vol. 6, Walter de Gruyter, Berlin, pp. 109-288, 1935.

C. André, Laboratoire d'Océanographie Dynamique et de Climatologie, CNRS/IRD/Université Pierre et Marie Curie, 4 Place Jussieu, Case 100, 75252 Paris Cedex 06, France.

E. S. Braga, Instituto Oceanográfico da Universidade de São Paulo, Praça do Oceanográfico, 191, São Paulo, SP, Brazil.

P. Morin, Centre National de la Recherche Scientifique, B.P. 74, 29682 Roscoff, France.

C. Oudot (corresponding author), Institut de Recherches pour le Développement, B.P. 70, 29280 Plouzané, France (oudot@ird.fr).

J.F. Ternon, Institut de Recherches pour le Développement, B.P. 165, 97323 Cayenne, French Guiana.

(Received April 7, 1998; revised March 29, 1999; accepted April 16, 1999.)